Swirling flow through a bend

By OSAMI KITOH

Department of Mechanical Engineering, Nagoya Institute of Technology,
Gokisocho, Showa-ku, Nagoya 466, Japan

An analytical study is made of a flow with swirling motion through a bend in a pipe with circular cross-section. The intensity of the swirl and the axial velocity distribution may change along a curved path according to the conservation law of angular momentum that is the basic principle used in this analysis. The analysis deals with the variation of angular-momentum flux components of the flow along the pipe. Approximate inviscid solutions indicate that, depending on the inlet conditions of the flow and the configuration of the bend, different types of swirling motion appear in the bend. The sign of a constant C appearing in the analysis is a governing parameter determining the flow type. Comparisons are made with the experimental results of other investigators. Finally, examples of swirling motion appearing in a real curved duct are discussed.

1. Introduction

Flow of a fluid in a curved duct has been the subject of much attention among investigators for its practical importance and scientific interest, and many valuable results have already been obtained. However, most of these results have been limited to cases in which fully developed flows were introduced into a single or composite bend.

In practice, however, flow approaching a bend is not always in a fully developed state, because it depends on the upstream conditions in the pipe. The flow into the bend may be associated with a swirling motion or shear component in axial velocity possibly as a result of fluid machines or spatially curved ducts ahead of the bend. The flow into an elbow-type draft tube of a water turbine working under partial load has an associated swirling component, and that is a primary reason for vibration of the draft tube as shown by Murakami (1961). Shimizu (1975) measured velocity distributions across the downstream section of multiple 90° bends and reported that, depending on the method of connecting the 90° bends upstream, there were various combinations of swirling and axial shear components. These additional flow components may alter the flow pattern from that of the well-known flow in a curved duct.

Binnie (1962) observed flow with a swirling motion through a bend and analysed the motion of a fluid particle that is in contact with the pipe wall. The particle motion would be periodic wavy or complete circular depending on the inlet conditions. Since Binnie's analysis was limited to flow adjacent to the wall, he gave no description of the flow field in the duct. Hawthorne (1951) indicated theoretically the appearance of secondary streamwise vorticity (swirling motion) along a curved streamline when initially there is a vorticity component normal to the streamwise direction. Applying this theory to a bend flow when the initial flow has uniform pressure and velocity varying in only one direction, he obtained a solution for secondary swirling motion

with its direction changing alternately along the bend. Similar procedures were developed by Horlock (1956) and Lakshminarayana & Horlock (1967) for flow through a bend or an axial-compressor cascade. Some success was achieved in predicting the flow field.

When the initial flow into a bend has a swirling component, however, it is difficult to analyse the flow using the method employed by Hawthorne for two reasons. First, a streamline of the flow is spiral along the pipe axis, and the principal normal of the streamline varies from place to place; it does not remain on the plane of curvature, whereas Hawthorne assumed it to be permanently on it. Secondly, the flow with the swirling component is associated with the streamwise vorticity. According to the present analysis, this vorticity component alters vorticity normal to the streamline, the effect of which cannot be neglected when one considers the swirling flow in the bend. This effect has not been taken into account in the Hawthorne-type analysis.

The present study develops an analytical approach to predict flow behaviour in a bend where there is initial swirling motion. The flow is formulated by use of the angular-momentum theory written in an integral form. The inviscid approximate solutions should help understanding of the qualitative nature of the flow in the bend. Experiments on swirling flow in a bend performed by Hawthorne (1951) when the initial flow was associated with an axial shear component and by Shimizu & Sugino (1980) when flow with a swirling component entered a bend are referred to for comparison with the predicted results. Some examples in the engineering field of swirling motion through a bend show aspects of flow behaviour similar to those predicted here.

2. Theory

A steady incompressible flow is assumed here. Fundamental equations that describe the flow in a curved duct are obtained by considering a conservation law of angular-momentum flux of the flow along the curved duct. Figure 1 shows the coordinate system employed in this study: θ is the angular position of a section measured from the bend inlet, and $\hat{r}$ and ϕ are the polar coordinates of a point within the section. The radii of curvature of the bend and of the pipe are $\hat{R}$ and $\hat{r}$, respectively. Figure 2 shows an elementary part of the bend whose deflection angle is $d\theta$ and the broken line denotes a control surface across which the balance of angular-momentum flux of the flow will be considered. Flow into the section where $\theta = \theta$, the upstream section of the control surface, generally has some angular-momentum flux. The definitions of the angular-momentum-flux components are illustrated in figure 3. In the cross-section considered, we introduce the P-axis in the plane of curvature and the N-axis perpendicular to it. The flux of angular momentum is resolved into three components: around the pipe axis, P-axis and N-axis respectively, which are expressed by the following formulae:

$$\hat{\Omega}(\theta) = \rho \int_0^{r_0} \int_0^{2\pi} \hat{V}_\phi \, \hat{V}_\theta \, \hat{r}^2 \, d\phi \, d\hat{r}, \tag{1}$$

$$\hat{\Lambda}(\theta) = \rho \int_0^{r_0} \int_0^{2\pi} \hat{V}_\theta^2 \, \hat{r}^2 \cos\phi \, d\phi \, d\hat{r}, \tag{2}$$

$$\hat{\Xi}(\theta) = \rho \int_0^{r_0} \int_0^{2\pi} \hat{V}_\theta^2 \, \hat{r}^2 \sin\phi \, d\phi \, d\hat{r}, \tag{3}$$
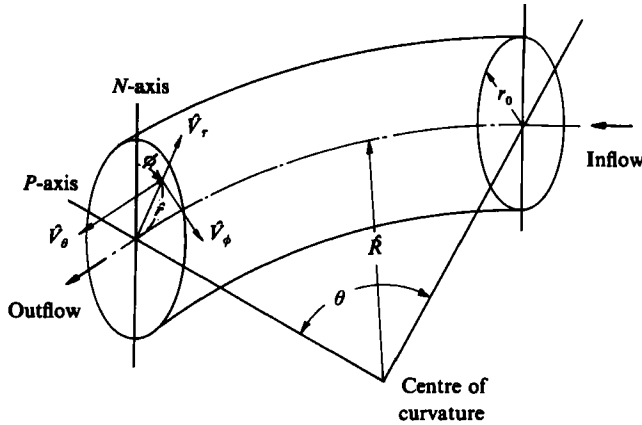
FIGURE 1. The coordinate system employed.
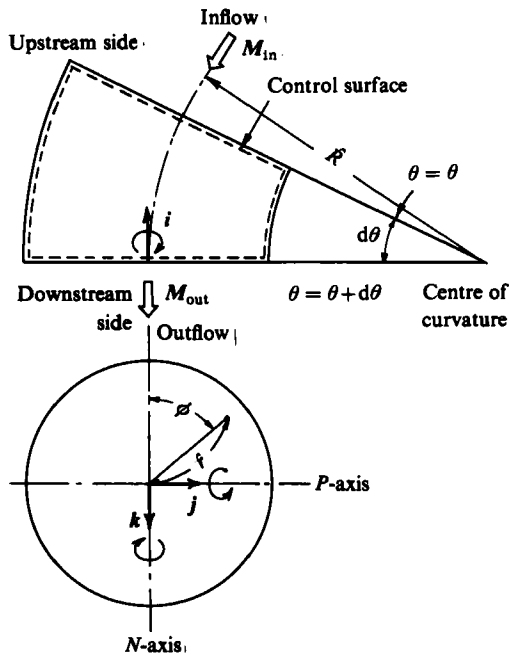
FIGURE 2. Elementary part of a bend having a deflection angle $d\theta$. The broken line denotes a control surface.

where $\hat{V}_\theta$ and $\hat{V}_\phi$ are axial and tangential velocity components and ρ is fluid density. $\hat{\Omega}$ relates to the swirling motion of the flow and is used as a parameter of the swirl intensity. The residual components $\hat{A}$ and $\hat{\Xi}$ relate to an uneven distribution of the axial velocity.

Since the downstream section of the control surface is inclined by $d\theta$ in the upstream section, the reference axes to calculate the angular-momentum flux differ at up- and downstream sections. In order to apply the momentum theory, a unification of the reference axes will be necessary. Here the axes at the downstream
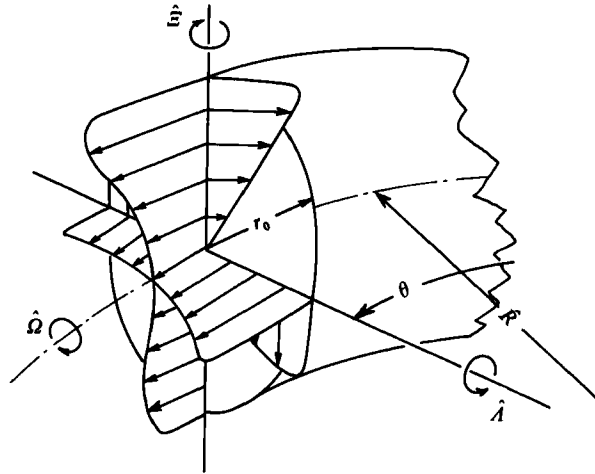
FIGURE 3. Definitions of angular-momentum-flux components $\hat{\Omega}$, $\hat{\Lambda}$ and $\hat{\Xi}$.

section will be chosen, so (1)–(3) for influx of the angular momentum at the section $\theta = \theta$ should be changed to those referring to new axes at $\theta = \theta + \mathrm{d}\theta$. Let unit vectors corresponding to the pipe axis, P-axis and N-axis at the downstream section be i, j and k respectively; then the angular momentum influx across the upstream section M_{in} can be written

$$M_{\mathrm{in}} = i(\hat{\Omega} - \hat{\Lambda}\,\mathrm{d}\theta) + j\left\{\left(-\rho\hat{R}\iint \hat{V}_\phi\,\hat{V}_\theta\,\hat{r}\,\sin\phi\,\mathrm{d}\phi\,\mathrm{d}\hat{r}\right.\right.$$
$$\left.\left. + \rho\hat{R}\iint \hat{V}_r\,\hat{V}_\theta\,\hat{r}\,\cos\phi\,\mathrm{d}\phi\,\mathrm{d}\hat{r} + \hat{\Omega}\right)\mathrm{d}\theta + \hat{\Lambda}\right\} + k\left\{\left(\rho\hat{R}\iint \hat{V}_\phi\,\hat{V}_\theta\,\hat{r}\,\cos\phi\,\mathrm{d}\phi\,\mathrm{d}\hat{r}\right.\right.$$
$$\left.\left. + \rho\hat{R}\int \hat{V}_r\,\hat{V}_\theta\,\hat{r}\,\sin\phi\,\mathrm{d}\phi\,\mathrm{d}\hat{r}\right)\mathrm{d}\theta + \hat{\Xi}\right\}, \quad (4)$$

where $\hat{V}_r$ is radial velocity. Similarly, the angular momentum efflux across the downstream section M_{out} can be written as

$$M_{\mathrm{out}} = i\left(\hat{\Omega} + \frac{\mathrm{d}\hat{\Omega}}{\mathrm{d}\theta}\,\mathrm{d}\theta\right) + j\left(\hat{\Lambda} + \frac{\mathrm{d}\hat{\Lambda}}{\mathrm{d}\theta}\,\mathrm{d}\theta\right) + k\left(\hat{\Xi} + \frac{\mathrm{d}\hat{\Xi}}{\mathrm{d}\theta}\,\mathrm{d}\theta\right). \quad (5)$$

Then the angular-momentum flux balance across the control surface becomes

$$M_{\mathrm{in}} - M_{\mathrm{out}} = i\left(-\frac{\mathrm{d}\hat{\Omega}}{\mathrm{d}\theta} - \hat{\Lambda}\right)\mathrm{d}\theta + j\left(-\rho\hat{R}\iint \hat{V}_\phi\,\hat{V}_\theta\,\hat{r}\,\sin\phi\,\mathrm{d}\phi\,\mathrm{d}\hat{r}\right.$$
$$\left. + \rho\hat{R}\iint \hat{V}_r\,\hat{V}_\theta\,\hat{r}\,\cos\phi\,\mathrm{d}\phi\,\mathrm{d}\hat{r} + \hat{\Omega} - \frac{\mathrm{d}\hat{\Lambda}}{\mathrm{d}\theta}\right)\mathrm{d}\theta + k\left(\rho\hat{R}\iint \hat{V}_\phi\,\hat{V}_\theta\,\hat{r}\,\cos\phi\,\mathrm{d}\phi\,\mathrm{d}\hat{r}\right.$$
$$\left. + \rho\hat{R}\iint \hat{V}_r\,\hat{V}_\theta\,\hat{r}\,\sin\phi\,\mathrm{d}\phi\,\mathrm{d}\hat{r} - \frac{\mathrm{d}\hat{\Xi}}{\mathrm{d}\theta}\right)\mathrm{d}\theta. \quad (6)$$

If the external force moment acting on the control surface is denoted by N, the following relation holds:

$$N + M_{\mathrm{in}} - M_{\mathrm{out}} = 0. \quad (7)$$

The external forces are exerted by pressure and friction forces acting on the control
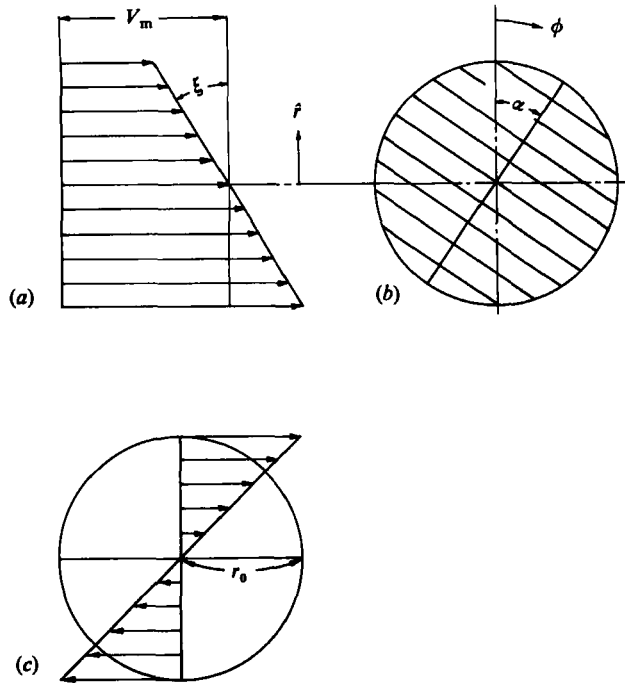
FIGURE 4. Flow model assumed here. (*a*) Axial velocity at $\phi = \alpha$; (*b*) equiaxial velocity contour; (*c*) tangential velocity profile (forced vortex).

surface of the fluid. In order to obtain approximate solutions, it is assumed that the flow is inviscid. Then the external torque can be expressed as

$$N = i\left(-\iint \hat{P} \cos\phi\, \hat{r}^2\, \mathrm{d}\phi\, \mathrm{d}\hat{r}\right)\mathrm{d}\theta + j\left(-\iint \frac{\partial \hat{P}}{\partial \theta} \cos\phi\, \hat{r}^2\, \mathrm{d}\phi\, \mathrm{d}\hat{r}\right)\mathrm{d}\theta$$
$$+ k\left(-\iint \frac{\partial \hat{P}}{\partial \theta} \sin\phi\, \hat{r}^2\, \mathrm{d}\phi\, \mathrm{d}\hat{r}\right)\mathrm{d}\theta, \quad (8)$$

where $\hat{P}$ is static pressure. The pressure acting on the bend wall $\hat{P}_{\mathrm{w}}$ contributes to the torque of the order of $(\mathrm{d}\theta)^2$. Because of its smallness it can be neglected.

3. Solutions obtained with a simple flow model

To obtain an approximate solution, a simple flow model is introduced. A flow with a forced-vortex-type swirling motion with a shear-type axial velocity is assumed. The model flow is illustrated in figure 4. This model is the same as the approximate solutions in Hawthorne's analysis. The velocity distributions of the model are expressed by

$$\left.\begin{array}{l} \hat{V}_\phi = \hat{r}\hat{\omega}, \\ \hat{V}_\theta = V_{\mathrm{m}} + \hat{r}\hat{\xi}\cos(\phi - \alpha), \end{array}\right\} \quad (9)$$

where V_{m} is the mean axial velocity and $\hat{\omega}$ is the angular velocity of the swirling motion. The angle α is the shear direction and $\hat{\xi}$ is the shear intensity of the axial velocity. Radial velocity is usually smaller than $\hat{V}_\theta$ or $\hat{V}_\phi$, and the contribution to the

angular-momentum-flux change may be so negligibly small that it can be neglected in the approximate solution.

For convenience, the following dimensionless variables are introduced:

$$\frac{\hat{\Omega}}{\rho \pi r_0^3 V_{\mathrm{m}}^2} = \Omega, \quad \frac{\hat{\Lambda}}{\rho \pi r_0^3 V_{\mathrm{m}}^2} = \Lambda, \quad \frac{\hat{\Xi}}{\rho \pi r_0^3 V_{\mathrm{m}}^2} = \Xi, \quad \frac{\hat{P}}{\frac{1}{2}\rho V_{\mathrm{m}}^2} = P, \quad \frac{\hat{r}}{r_0} = r, \quad \frac{\hat{R}}{r_0} = R.$$

Now substitution of (9) into (1)–(3) gives the relations

$$\left.\begin{aligned} \Omega &= \tfrac{1}{2}\omega, \\ \Lambda &= \tfrac{1}{2}\xi \cos\alpha, \\ \Xi &= \tfrac{1}{2}\xi \sin\alpha, \end{aligned}\right\} \tag{10}$$

where $\xi = \hat{\xi}/(V_{\mathrm{m}}/r_0)$ and $\omega = \hat{\omega}/(V_{\mathrm{m}}/r_0)$.

Although the real velocity distribution appearing in the actual physical systems is not exactly the same as the assumed one, averaged properties of the flow across the section would be similar if the flux of angular momentums were the same.

Euler's equation of motion in the r-direction,

$$\hat{V}_r \frac{\partial V_r}{\partial \hat{r}} + \frac{\hat{V}_\phi}{\hat{r}}\frac{\partial \hat{V}_r}{\partial \phi} + \frac{\hat{V}_\phi}{(\hat{R}-\hat{r}\sin\phi)}\frac{\partial \hat{V}_r}{\partial \theta} - \frac{\hat{V}_\phi^2}{\hat{r}} - \frac{V_\theta^2 \sin\phi}{(\hat{R}-\hat{r}\sin\phi)} = -\frac{\partial}{\partial \hat{r}}\left(\frac{\hat{P}}{\rho}\right), \tag{11}$$

gives the pressure distribution in the cross-section if the relationship of (9) is introduced, and an integration is performed over the section with respect to $\hat{r}$. Let $\hat{P}_0$ be the pressure at the centre of the duct, then

$$\frac{\hat{P}-\hat{P}_0}{\rho} = \tfrac{1}{2}\hat{r}^2 \hat{\omega}^2 + \left(V_{\mathrm{m}} + \frac{\hat{R}\hat{\xi}\cos(\phi-\alpha)}{\sin\phi}\right)^2 \ln\left(1 - \frac{\hat{r}}{\hat{R}}\sin\phi\right)$$

$$+ \hat{r}\hat{\xi}\cos(\phi-\alpha)\left(2V_{\mathrm{m}} + \frac{\hat{R}\hat{\xi}\cos(\phi-\alpha)}{\sin\phi}\right) + \tfrac{1}{2}\hat{r}^2\hat{\xi}^2 \cos^2(\phi-\alpha). \tag{12}$$

If (9), (10) and (12) are substituted into (7) and the analysis is confined to a bend with a larger radius of curvature than r_0, the momentum equations reduce to

$$\frac{\mathrm{d}\Omega}{\mathrm{d}\theta} = \quad -\Lambda \tag{13}$$

$$\frac{\mathrm{d}\Lambda}{\mathrm{d}\theta} = \quad \Omega \qquad -R\Omega\Xi \tag{14}$$

$$\frac{\mathrm{d}\Xi}{\mathrm{d}\theta} = \qquad\qquad R\Omega\Lambda \tag{15}$$

These differential equations govern the variations of angular momentum flux along the curved duct. Equation (13) can be written, taking the axial vorticity $\omega_\theta = 2\omega$, as

$$\frac{\mathrm{d}\omega_\theta}{\mathrm{d}\theta} = -2\xi \cos\alpha. \tag{16}$$

This equation is the same as (14) in Hawthorne's report, which describes the generation of streamwise vorticity along a curved path when there is vorticity normal to the streamline. Equations (14) and (15) are the additional dynamic relations
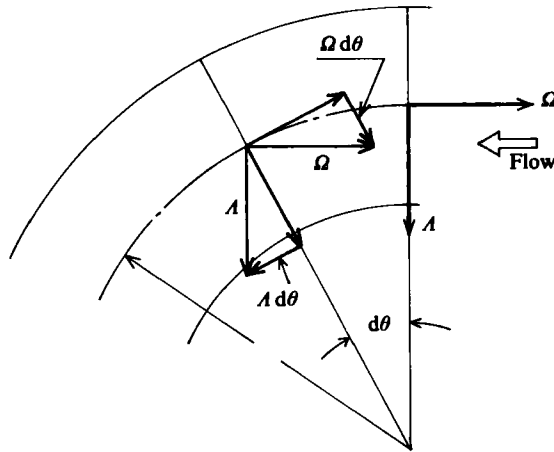
FIGURE 5. Angular-momentum-flux components Ω and Λ evaluated at two different reference axes. In the initial section they are Ω and Λ, but in the downstream section additional terms $-\Lambda d\theta$ and $\Omega d\theta$ appear that are part of the variation of these components, group I in (13) and (14).
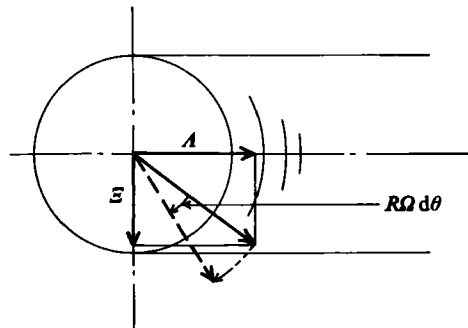
FIGURE 6. Rotation of vector components Λ and Ξ by a swirling motion which causes variation of these components, group II in (14) and (15).

needed to describe the flow in the bend. These equations indicate that the mutual interactions among angular-momentum-flux components of flow in a bend are essential to understand the characteristic features of the flow.

Equations (13)–(15) can be understood intuitively from another point of view. The variations of angular-momentum-flux components along a curved path are interpreted as a sum of two basic contributions. In the equations, the right-hand-side terms are separated into two groups I and II, as enclosed by the broken lines. Group I describes the variations of the vector components lying on the curvature plane (Ω and Λ) as a result of the rotation of the reference axes. As shown schematically in figure 5, these components, Ω and Λ in the upstream section, have additional components $-\Lambda d\theta$ and $\Omega d\theta$ when referred to a new coordinate, $d\theta$ downstream section. Group II describes the contribution of rotation of the vector components lying within the cross-sectional surface of the bend (Λ and Ξ) by the swirling velocity, as is shown in figure 6. The rotation angle can be calculated as $R\Omega\,d\theta$ within the mean axial flow, subtending an arc length of $Rd\theta$. This rotation of the vector causes variations in the vector components of $-R\Omega\Xi\,d\theta$ or $R\Omega\Lambda\,d\theta$ respectively.
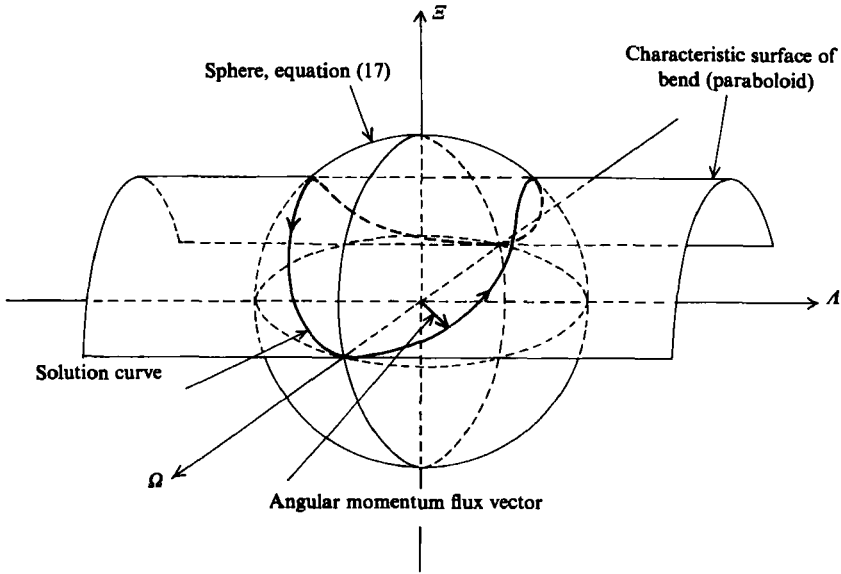
FIGURE 7. Two integral surfaces of differential equations, sphere and paraboloid, and a solution curve determined as an intersection of these surfaces.

To study the general properties of the equations, two integrals are derived. By eliminating R, the following relation is obtained as a first integral:

$$\Omega^2 + \Lambda^2 + \Xi^2 = C_1^2, \tag{17}$$

where $C_1 = (\Omega_0^2 + \Lambda_0^2 + \Xi_0^2)^{\frac{1}{2}} = $ const. is the integral constant. The suffix zero attached to any variable shows the value evaluated at the bend inlet section. Thus, the sum of the squares of the angular-momentum-flux components is an invariant of the flow. This conclusion should not be confused with the usual conservation law of angular-momentum flux, for in this analysis a local coordinate system is adopted instead of an absolute one. The implication of the relation is that the angular-momentum-flux vector M should exist on a spherical surface of radius C_1 in (Ω, Λ, Ξ)-space, as shown in figure 7. The second integral is obtained by eliminating Λ from (13) and (15), and the result is

$$\Xi + \tfrac{1}{2} R\Omega^2 = C_2, \tag{18}$$

where $C_2 = \Xi_0 + \tfrac{1}{2} R\Omega_0^2 = $ const. is the integral constant, which can be considered as a second invariant of the flow. The values C_1 and C_2 are determined from the inlet flow conditions into the bend. The parabolic relation between Ω and Ξ, (18), is also drawn in figure 7. The shape of the parabolic surface is determined only if the bend radius R is given while the vertical position along Ξ-axis depends on the inlet flow conditions. Thus the shape of the paraboloid can be considered as the characteristic one for a bend having radius of curvature R. The solution curve is given as the intersection of the sphere and the paraboloid, an example of which is given in the figure. It is convenient to project the curves onto a (Ω, Ξ)-plane to clarify the overall behaviour of the solution curves. In this plane five relative configurations between a parabola and a circle are possible, as shown in figure 8. A particular solution corresponds to each configuration. In what follows, we shall discuss the characteristics of each solution and the corresponding physical flow characteristics appearing in the bend.
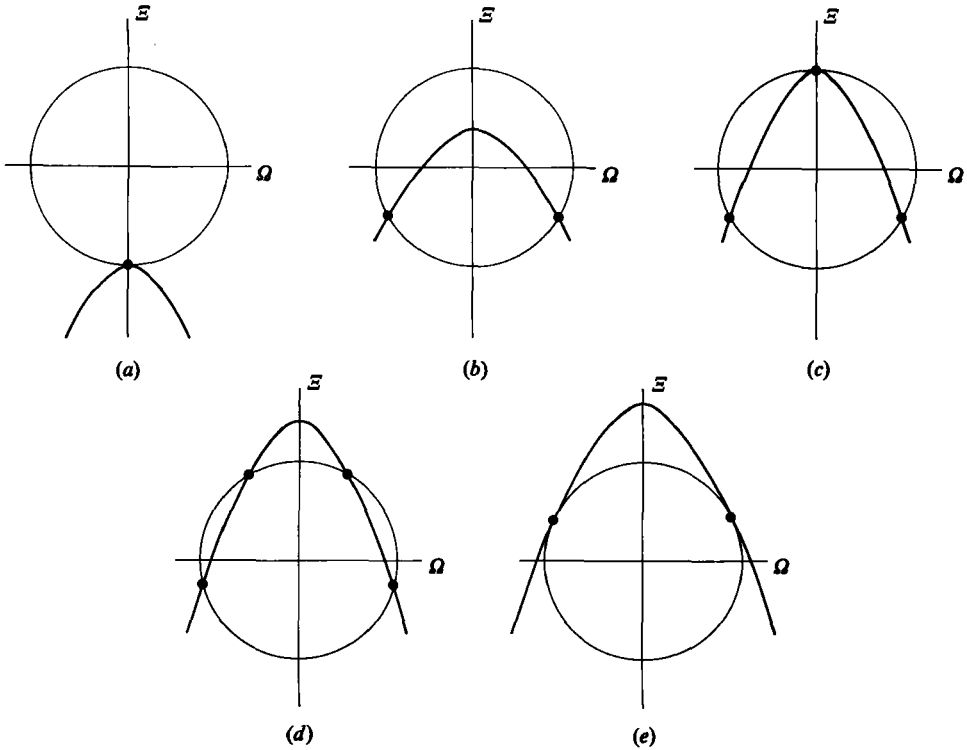
FIGURE 8. Solution curve projected onto the (Ω, Ξ)-plane, showing five relative positions between circle and parabola.

First consider case (a) when there is one tangential contact point between two curves. The solution curve reduces to a point $(\Omega = \Lambda = 0, \Xi < 0)$, which corresponds to a singular point of the differential equations, and the flow pattern does not change along the curved path. A flow having higher axial velocity on the outer side of a bend duct $(\Xi_0 < 0)$ is simulated by this case. Because this configuration of axial velocity generates a stable stratification of the centrifugal force, no further change in the motion is expected, as the theory predicts.

In case (b), there are two intersection points. This case is realized when the apex of the parabola exists within the interior region of the circle, i.e. when the following relation is satisfied:

$$(\Omega_0^2 + \Lambda_0^2 + \Xi_0^2)^{\frac{1}{2}} > |\Xi_0 + \tfrac{1}{2}R\Omega_0^2|, \tag{19}$$

or if a new parameter C is introduced,

$$C = \Omega_0^2 + \Lambda_0^2 + \Xi_0^2 - (\Xi_0 + \tfrac{1}{2}R\Omega_0^2)^2, \tag{20}$$

then $C > 0$. In figure 9, the solution curves projected onto the (Ω, Λ)-plane are shown. The curves are drawn with C_1 constant and C_2 having two values of different sign. When the apex of the parabola lies within the lower semicircular, negative region of Ξ, the curve has an elliptical shape, while it deforms into a butterfly form concaved in the Λ-axis direction in the other case. In either case, when the inlet state is S_0, for example, as the flow proceeds through the bend duct, θ increases, Ω and Λ follow the curve in the direction indicated by an arrow. The sign of Ω changes along the
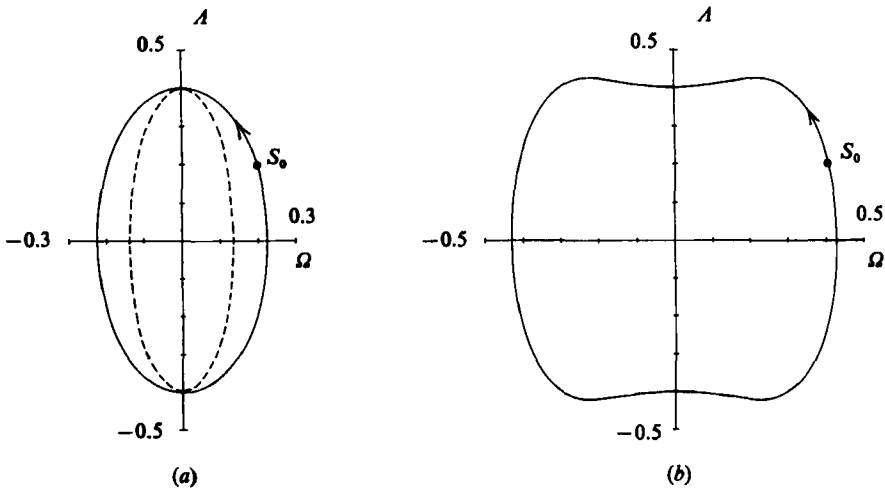
FIGURE 9. Solution curves projected onto the (Ω, Λ)-plane when C is positive. $R = 6$, $C_1 = 0.5$: (a) $C_2 = -0.3$; (b) $C_2 = 0.3$. Broken line is for the case $R = 20$.
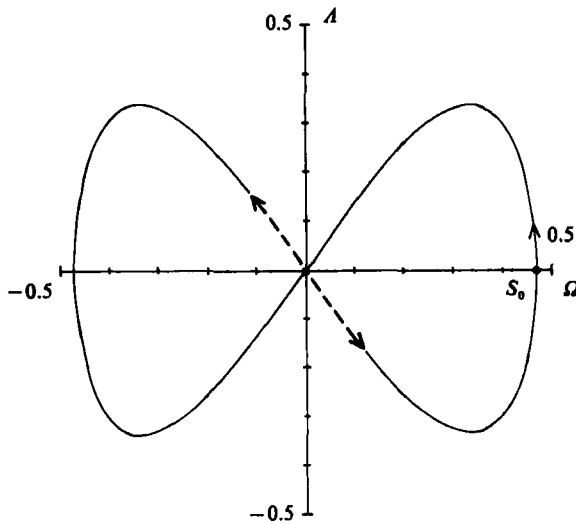
FIGURE 10. Solution curve projected onto the (Ω, Λ)-plane when C is zero. $R = 6$, $C_1 = 0.5$, $C_2 = 0.5$.

curve, so a swirling motion with its direction changing alternately appears in the bend.

A typical example of case (b) is a Hawthorne-type inlet flow, $(\Omega_0 = \Xi_0 = 0,$ $\Lambda_0 \neq 0)$, i.e. initially with velocity varying only in N-axis direction. The apex of the parabola exists at the origin in this case, and the experimental results show that the swirling motion with alternately changing direction appears, as predicted here.

As the radius of curvature of the bend increases, the shape of the solution curve becomes slender as shown by the broken line in the figure, and the secondary swirling becomes weak. Hence, the effect of the existence of the swirling component (streamwise vorticity) on the variation of the vorticity normal to the streamline,

which was neglected in Hawthorne's analysis as mentioned in §1, becomes less important for large R. This point will be discussed in detail in §5.

In case (c) there exist two intersection points and one tangential contact point. This solution is obtained when $C = 0$. The solution curve projected onto the (Ω, Λ)-plane is shown in figure 10. The characteristic feature of the curve is that it passes through the origin. When an initial flow into a bend is denoted by S_0, Ω and Λ follow the curve in the arrow direction and proceed to the origin ($\Omega = \Lambda = 0$). To reach the origin from the starting point S_0, an inifinitely large deflection angle of the bend is required, for near the origin the deflection angle can be expressed as

$$\theta = -\frac{1}{(RC_2 - 1)^{\frac{1}{2}}} \ln \Omega + A, \tag{21}$$

where A is constant. This relation indicates that the state represented by the origin can never be attained in a real bend. Thus a gradually terminating swirling motion appears in the bend. Of particular interest is the case with an initial flow having a higher axial velocity on the inner side of the bend ($\Omega_0 = \Lambda_0 = 0$, $\varXi > 0$), i.e. the origin corresponds to the initial state. This flow condition corresponds to a singular point and is neutrally unstable with respect to a small disturbance, in contrast to case (a). A swirling flow in the clockwise or counterclockwise direction appears in the downstream section depending on the nature of the disturbance, as shown by the dotted line and arrows in the figure. Because this configuration of the initial axial velocity is unstable, it is soon replaced by the Dean-type double spirals that usually occur in a bend. In a sharply curved bend, however, there is not enough time for the Dean-type secondary flow to develop, and the potential vortex ($\varXi > 0$) appearing in the inlet region of the bend would be followed by a swirling motion in the downstream section.

Tunstall & Harvey (1968) observed a single circulation about the axis (swirling motion) in either a clockwise or counterclockwise direction in the downstream section of a mitred right-angle bend. The direction of swirl changes at a low frequency. They explained that a large-scale turbulent vorticity flowing into the bend switched the direction, which can be considered one of the disturbances as described above.

In case (d) there are four intersection points. The apex of the parabola exists outside the circle, and this situation would be obtained when $C < 0$. Initial swirling motion ($\Omega_0 \neq 0$) is inevitable to realize this type of flow as is easily seen from (20). The solution curves projected on the (Ω, Λ)-plane are shown in figure 11. Two separate curves appear, and which one is the solution curve depends on whether the initial swirling component Ω is positive or negative. The values of Ω and Λ follow the curve in the counterclockwise direction as θ increases. In this case the solution curves do not pass through the line $\Omega = 0$, so the swirl direction remains unchanged through the bend. If an initial flow has only a swirling component ($\Omega_0 \neq 0$, $\Lambda_0 = \varXi_0 = 0$), and an inequality relation $1/2R\Omega_0^2 \gg |\Omega_0|$ holds, the solution curves reduce to two points. Thus, for a bend having large R, a swirling motion can pass through it without undergoing any change.

In the last case, (e), there are two tangential contact points. This particular case is obtained when $\Lambda_0 = 0$ and $\varXi_0 = 1/R$, and these points are singular points. Thus, the initial flow remains unchanged through the bend. To the author's knowledge, this type of flow has not been reported before.

From the above considerations it is concluded that the sign of the constant C or the relative position of the apex of the parabola with respect to the circle, which is
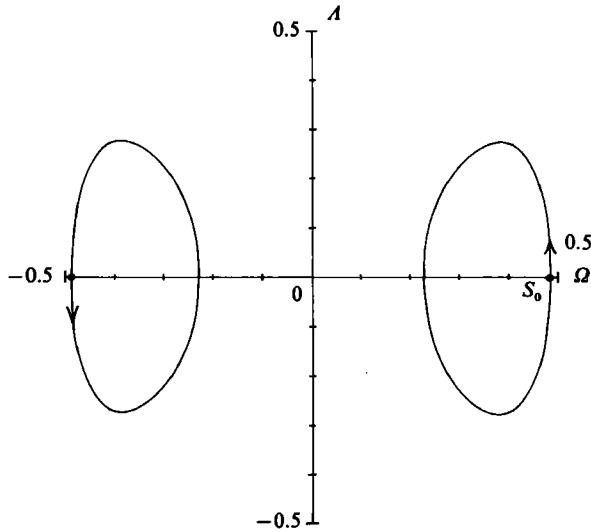
FIGURE 11. Solution curves projected onto the (Ω, Λ)-plane when C is negative. $R = 6$,
$C_1 = 0.5$, $C_2 = 0.6$.
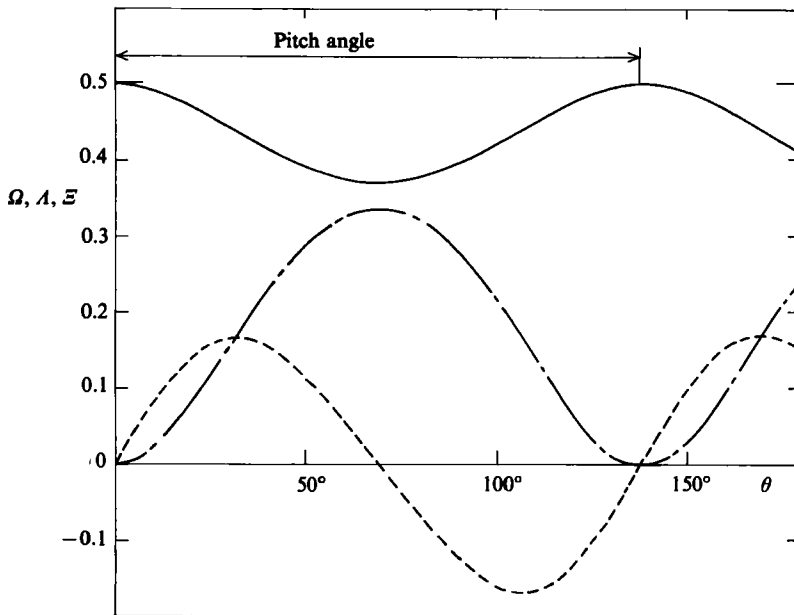
FIGURE 12. Variation of angular-momentum-flux components Ω, Λ, and Ξ against θ when an initial
flow with $\Omega_0 = 0.5$ and $\Lambda_0 = \Xi_0 = 0$ enters a bend of $R = 6$: ———, Ω; — — — —, Λ; — · — · —, Ξ.

determined from the initial flow and the bend geometry, is a factor determining what
kind of swirling motion would appear in a bend.

Figure 12 shows an example of variation of angular-momentum-flux components
with θ. The swirl intensity Ω as well as other components shows sinuous variation
along θ except for the gradually terminating case. The pitch of these curves differs
from case to case. The pitch angle θ_p is estimated from (13) as

$$\mathrm{d}\theta = -\mathrm{d}\Omega/\Lambda.$$
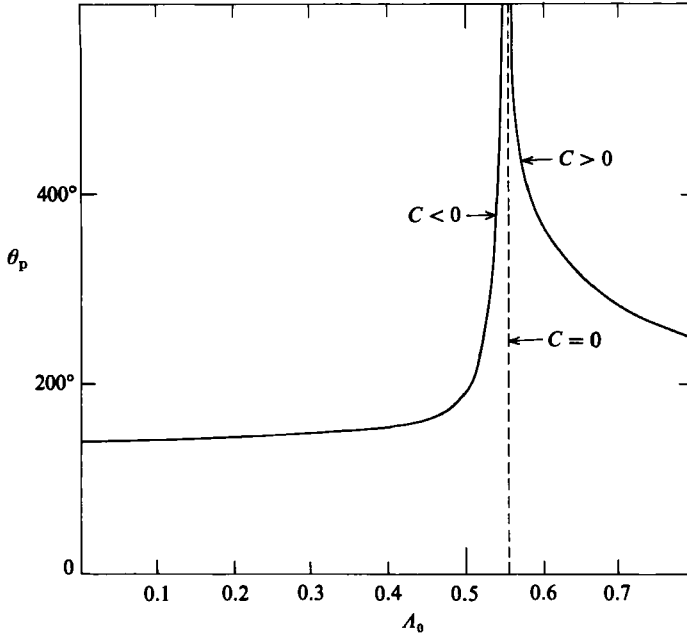
FIGURE 13. Pitch angle of wave in angular-momentum-flux curves. $\Omega_0 = 0.5$, $\Xi_0 = 0$, $R = 6$.

Therefore
$$\theta_p = -\frac{2}{R}\oint \frac{d\Omega}{\pm\left(\Omega^4 - 4/R_4\left(1 - RC_2\right)\Omega^2 + 4C/R^2\right)^{\frac{1}{2}}}. \tag{22}$$

Integrating this relation gives the following expressions for θ_p.

For $C > 0$

$$\theta_p = \frac{8}{R}\frac{1}{(a^2+b^2)^{\frac{1}{2}}}K\left(\frac{a}{(a^2+b^2)^{\frac{1}{2}}}\right), \tag{23}$$

and $C < 0$

$$\theta_p = \frac{4}{aR}K\left(\frac{(a^2-b^2)^{\frac{1}{2}}}{a}\right), \tag{24}$$

where

$$a^2 = -\frac{2(1-RC_2)}{R^2} + \left[\left(\frac{2(1-RC_2)}{R^2}\right)^2 + \frac{4C}{R^2}\right]^{\frac{1}{2}}$$

and

$$b^2 = \frac{2(1-RC_2)}{R^2} + \left[\left(\frac{2(1-RC_2)}{R^2}\right)^2 + \frac{4C}{R^2}\right]^{\frac{1}{2}}.$$

The function $K(k)$ denotes a complete elliptic integral of the first kind. Figure 13 shows the variation of the pitch angle when the initial angular-momentum-flux component Ω_0 is kept constant and A_0 is varied. When C is positive, θ_p decreases as A_0 increases but it increases when C is negative. At the point where C becomes zero, θ_p becomes infinite.

4. Comparison with experimental results

Experimental results for swirling flow in a bend performed by other investigators will be compared with the predicted results given in the previous section. Hawthorne (1951) made measurements of total-pressure distributions of flow in a bend with radius of curvature $10r_0$, when the inlet flow is of uniform pressure with a velocity
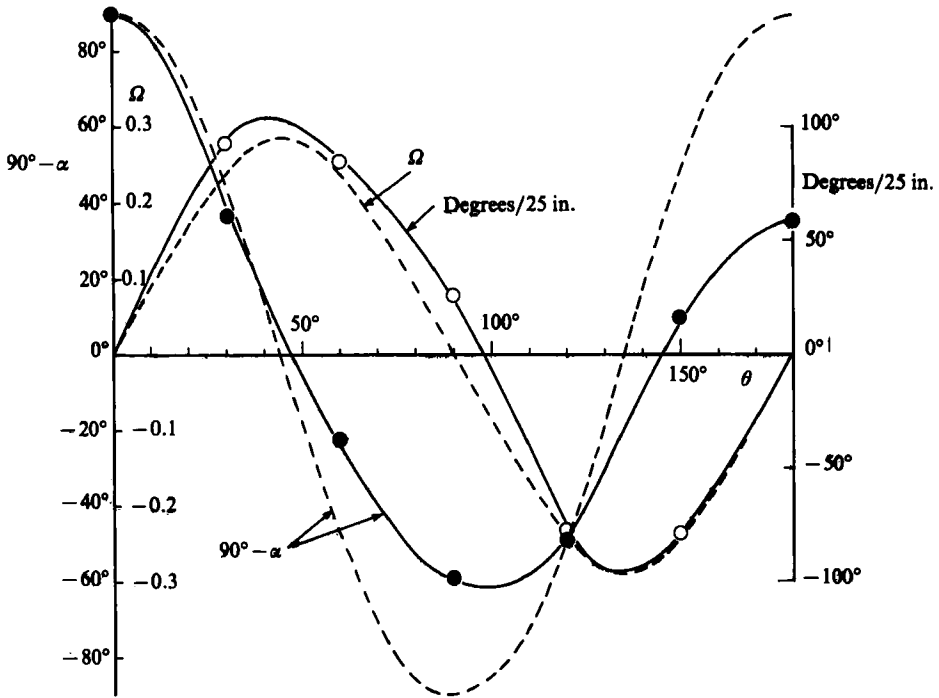
FIGURE 14. Comparison with measured results of Hawthorne when an initial flow with $\Omega_0 = \Xi_0 = 0$ and $\Lambda_0 = -0.5$ enters a bend of $R = 10$: ●, shear direction of axial velocity; ○, twisting angle per 25 in. of straight pipe due to secondary circulating motion; – – – –, predicted results for shear direction and swirl intensity.

varying in one direction only. From the measured total-pressure distributions, the shear angle α and the twist angle due to the secondary swirling motion were estimated. The results are given in figure 14. The results predicted by the present method for the same initial conditions are shown by broken lines. Here the definition of shear angle α is in agreement with Hawthorne. Since the intensity of the secondary swirling motion was represented by a twist angle per 25 in. of straight pipe but not by swirl intensity itself in his study, it is impossible to expect an exact correspondence between them. But the trend of the predicted curves is the same as the measured ones, thus confirming the analysis in this case as being correct.

Shimizu & Sugino (1980) measured velocity distributions in a bend duct with a radius of curvature $6r_0$, when a flow with a swirling component entered the bend. Figure 15 shows the measured variations of the swirl intensity along the deflection angle. When flow with an intensive swirl component enters the bend, the sign of Ω does not change and shows only a wavy variation along θ. The pitch of this wavy curve becomes small as the intensity of the inlet swirl is increased. When flow with a weak swirl component enters the bend, the swirl intensity decreases monotonically and finally changes its sign, although the deflection angle of the bend is too short to attain this state in this case. The predicted results corresponding with the above initial conditions are given by broken lines in the figure; they indicate a tendency similar to the measured one, although the wave pitch shows some disagreement, possibly caused to a great degree by a frictional effect on the momentum balance, which is neglected in the approximate solutions. To obtain a quantitative agreement,
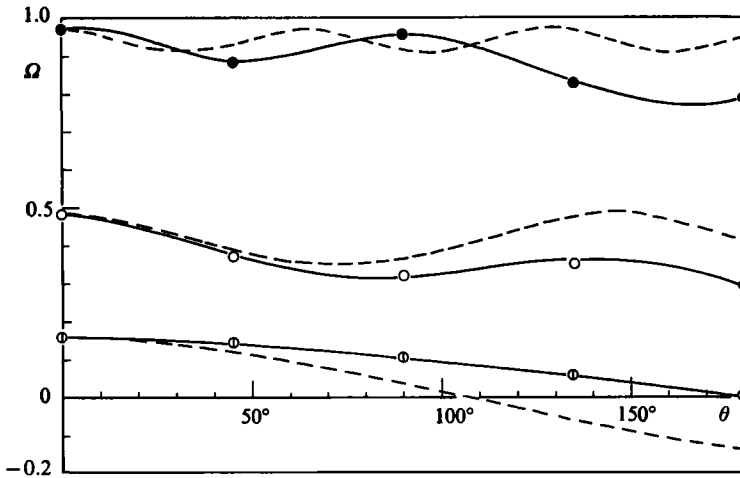
FIGURE 15. Comparison with swirl intensity measured by Shimizu & Sugino with bend of $R = 6$: ●, $\Omega_0 = 0.971$, $\Lambda_0 = \Xi_0 = 0$; ○, $\Omega_0 = 0.483$, $\Lambda_0 = \Xi_0 = 0$; ⊕, $\Omega_0 = 0.159$, $\Lambda_0 = \Xi_0 = 0$; ----, predicted swirl intensity for the same initial conditions as in the experiment.
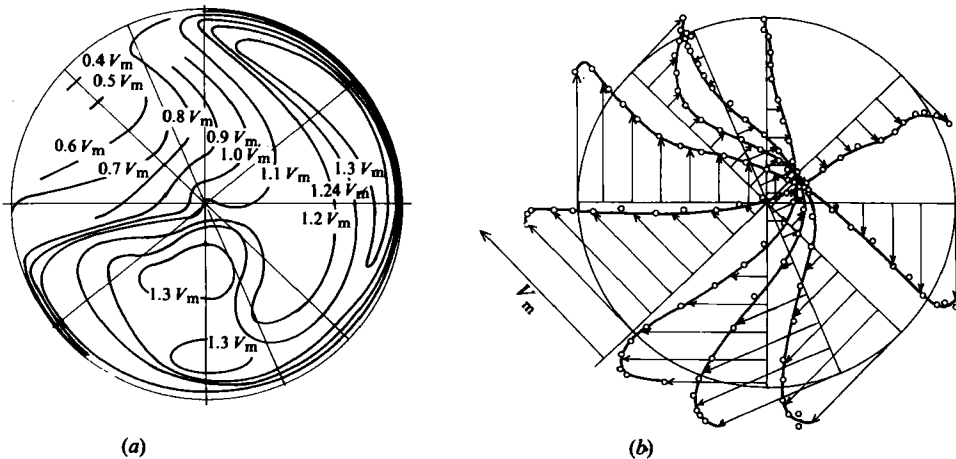
FIGURE 16. Axial and tangential velocity distributions in a $1.6r_0$ downstream section of a second bend with a connecting angle $\phi = 120°$, after Shimizu (1975). (a) Axial velocity; (b) tangential velocity.

it would be necessary to consider the effect of secondary flow of Dean-type double spirals on the velocity distributions, in addition to the effect of friction, the development of which cannot be predicted by the present method.

5. Swirling motion in real curved duct

In triply connected 90° bends, the loss of head along the bends has a complicated form depending on the manner in which the bends are connected. Measurements made by Shimizu (1975) showed that the bend loss varies from two to five times that of a single 90° bend loss. He also indicated from detailed velocity measurements that
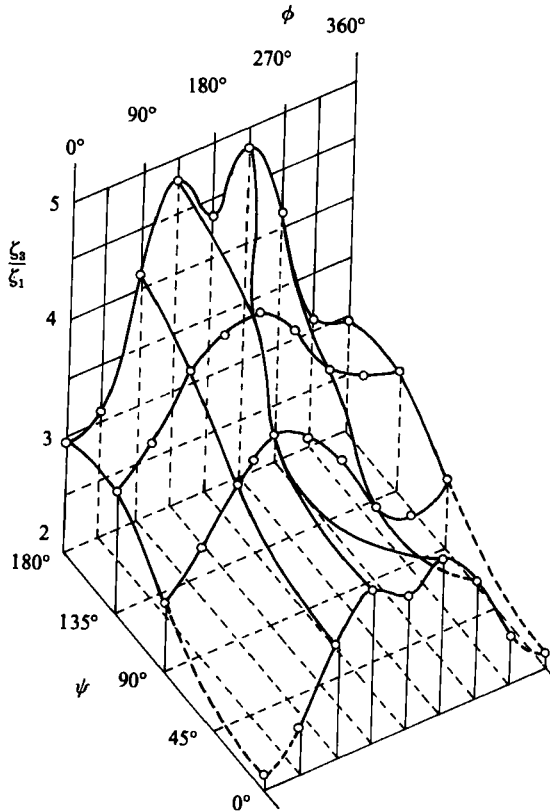
FIGURE 17. Total loss of triply connected 90° bends ζ_3 relative to that of a single 90° bend ζ_1 as a function of connecting angles ϕ and ψ after Shimizu (1975).

the swirling motion and the uneven axial velocity appearing in the bend duct have primary effects on the bend loss.

In the first bend, Dean-type secondary motion appears and a shear axial velocity results. If a second bend is connected that is non-coplanar with the first one, angle ϕ between them, the axial shear component produces a swirling component in the downstream section of the bend, as does Hawthorne-type flow. Figure 16 shows an example, measured at the $1.6r_0$ downstream section of the second bend by Shimizu. Single swirling motion, although not axisymmetry, with axial shear component is the characteristic feature of the velocity distribution at this section. If these components enter a third bend, generally non-coplanar with the former bends, making angle ψ with the second bend, their intensities are varied in the bend by the mechanism described here. The resultant swirling intensity at the bend exit has an intimate relation with the bend loss, and the total loss becomes a complicated function of the connecting angles ϕ and ψ, as shown in figure 17.

Flow in a draft tube of a water turbine operating under partial load is accompanied by a swirling motion. Murakami (1961) suggested that such swirling motion causes a vibration of the draft tube as a result of whirling motion of the swirling axis in the tube. The whirling frequency is determined as a function of the swirl intensity. Uneven efflux of momentum from the draft tube due to the whirling motion is the origin of the exciting force. A bend-type draft tube is commonly used for geometric
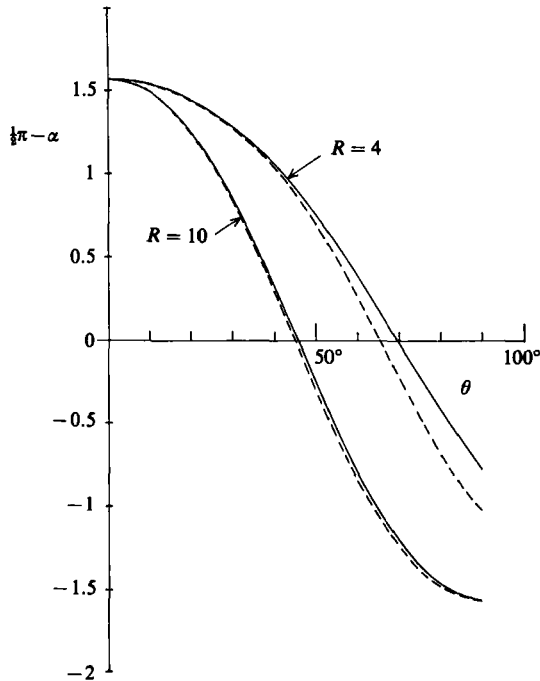
FIGURE 18. Effect of swirling motion on prediction of swirl intensity: ——, neglected, using equation (18) in Hawthorne's paper; – – – – included, based on the present analysis.

reasons and the swirling motion is subjected to the influence of the curvature of the duct. Thus a change in vibrating frequency of the draft tube is expected if the bend geometry is varied. In fact, Murakami pointed out that the frequency varies when the radius of curvature of the bend R is increased from 3 to 6. This variation would have some relation with the phenomena considered here.

If we consider only one half (upper or lower half) of a section of a bend with a circular cross-section, the final state of the bend flow would be a single vortex (swirling motion) instead of Dean-type double vortex. In this case, the fully developed initial flow has the Λ_0 component of angular momentum flux associated with it. According to the present analysis, this type of flow is converted into a periodic swirling flow of Hawthorne type, although the analysis should be modified for the semicircular section. Before the secondary swirling motion attains its final state, some aspect of the periodicity would be observed in a real bend. Energy loss across the bend is one example showing the wavy variation as pointed out by Hawthorne (1951). Choi, Talbot & Cornet (1979) measured wall shear stresses in the entry region of a curved tube having $R = 7$ and indicated that the averaged shear stress around the periphery shows some wavy variation along downstream direction. These phenomena undoubtedly have an intimate relation with the suggestion made by Rowe (1970) that the secondary circulation does not grow monotonically but shows some wavy variation.

It is worth noting that the relative importance of the first term with respect to the second one on the right-hand side of (14) becomes significant when $R|\Xi| \ll 1$. This term describes the effect of swirling motion Ω (streamwise vorticity) on the variation of Λ (vorticity normal to the streamline) that is neglected in the Hawthorne-type analysis. In a flow passing through a strongly curved bend, i.e. small R, or having

a dominant swirling component, $|\Omega| \gg |\Xi|$, this term plays an essential role in the variation of Λ. Neglecting the term results in a serious error in flow prediction. When an initial flow contains only a swirling component, the analysis neglecting the term fails completely to predict the variation of the swirl intensity in the duct. Even in Hawthorne-type initial flow, $\Lambda_0 \neq 0$, the effect becomes large as R decreases. Figure 18 compares the results based on two analyses, either considering or neglecting the swirling-motion effect. When $R = 10$, no appreciably difference can be seen between them, but it becomes noticeable when R is reduced to 4. For a flow in a bend or turbomachinery cascade that has a relatively small R (not rare in engineering practice) neglect of the effect would lead to some error in predicting the flow.

REFERENCES

BINNIE, A. M. 1962 Experiments on the swirling flow of water in a vertical pipe and bend. *Proc. R. Soc. Lond.* A**270**, 452.

CHOI, U. S., TALBOT, L. & CORNET, I. 1979 Experimental study of wall shear rates in the entry region of a curved tube. *J. Fluid Mech.* **93**, 465.

HAWTHORNE, W. R. 1951 Secondary circulation of fluid flow. *Proc. R. Soc. Lond.* A**206**, 374.

HORLOCK, J. H. 1956 Some experiments on the secondary flow in pipe bend. *Proc. R. Soc. Lond.* A**234**, 335.

LAKSHMINARAYANA, B. & HORLOCK, J. H. 1967 Effect of shear flows on the outlet angle in axial compressor cascade – method of prediction and correlation with experiments. *Trans. ASME.* D: *J. Basic Engng* **89**, 191.

MURAKAMI, M. 1961 Vibration of water-turbine draft tubes. *Trans. ASME.* A: *J. Engng for Power* **83**, 36.

ROWE, M. 1970 Measurements and computation of flow in pipe bends. *J. Fluid Mech.* **43**, 771.

SHIMIZU, Y. 1975 Flow and loss of multiple bends. Dissertation, Nagoya University.

SHIMIZU, Y. & SUGINO, K. 1980 Hydraulic losses and flow patterns of a swirling flow in U-bends. *Bull. JSME* **23**, 1443.

TUNSTALL, M. & HARVEY, J. K. 1968 On the effect of sharp bend in a fully developed turbulent pipe-flow. *J. Fluid Mech.* **34**, 595.